23rd ABCM International Congress of Mechanical Engineering
December 6-11, 2015, Rio de Janeiro, RJ, Brazil

CFD SIMULATION OF A BUBBLING FLUIDIZED BED USING LATTICE BOLTZMANN BASED DRAG MODELS

Carlos Manuel Romero Luna
Ivonete Ávila
UNESP - Univ Estadual Paulista, Faculty of Engineering at Guaratinguetá, Department of Energy, Av. Dr. Ariberto Pereira da Cunha, 333 - 12.516-410, Guaratinguetá-SP, Brazil
c_romeroluna@yahoo.com; iavila@unesp.br

Gretta Larisa Aurora Arce Ferrufino
National Institute For Space Research, Combustion and Propulsion Associated Laboratory, Rodovia Presidentre Dutra, km 40, Cachoeira Paulista-SP, Brazil.
gretta@lcp.inpe.br

Abstract

In Computational Fluid Dynamics (CFD) simulations of fluidized beds, the description of gas-solid flow hydrodynamics relies of a drag model to account the momentum transfer between the gas and solid phases. Different studies about drag models have been reported in the literature. However, there are few studies concerning drag models derived from Lattice Boltzmann (LB) simulations applied to a bubbling fluidized bed. This work provides a comprehensive study of drag models derived from Lattice Boltzmann simulations reported in the literature, in order to assess their performance in simulating gas-solid flow hydrodynamics in a bubbling fluidized bed. A CFD model using the MFIX code based on the Eulerian-Eulerian approach considering the KTGF was used to simulate a 2D bubbling fluidized bed with Geldart B particles. The simulation results are validated with the experimental data from Jung et al. (2005). From the results it can be concluded that the LB drag models has the same ability to predict the gas-solid hydrodynamics in a bubbling fluidized bed that drag models obtained from experimental tests.

Keywords: CFD, bubbling fluidized bed, Lattice Boltzmann drag models,

1. INTRODUCTION

Fluidized beds are extensively used in many industries including chemicals, petroleum, mining, pharmaceuticals, and energy. Fluidized beds are used due to the high mixing between the gas and solid phases, this enhances chemical reactions and produces high rates of heat and mass transfer. Some of the major applications include fluid catalytic cracking (FCC), combustion, gasification, pyrolysis, polymerization, fuel synthesis, coating, roasting, and heat exchangers (Gupta and Sathiyamoorthy, 1999; Kunii and Levenspiel, 1991; Oka and Anthony, 2004; Zimmermann and Taghipour, 2005; Schreiber et al., 2011). The performance of these applications mainly depends on a suitable understanding of gas-solid flow hydrodynamics, which has a governing effect on the overall heat and mass transfer processes occurring in the fluidized bed. Thus, understanding the gas-solid hydrodynamics helps to the design, scale-up, and optimization of industrial-scale units.

Nowadays, Computational Fluid Dynamics (CFD) has become a powerful tool to study the gas-solid flow hydrodynamics in fluidized beds (Armstrong, Gu and Luo 2010). There are two main approaches used in CFD modeling of gas-solid flow, the Eulerian–Lagrangian approach, which is also referred to as the discrete particle model (DMP) and the Eulerian-Eulerian approach, or also called as two-fluid model (TFM) (Deen, Van Sint Annaland, Van der Hoef, & Kuipers, 2007; Vejahati et al., 2009). However, comparing these two approaches, due to the high computational time consumption for the Eulerian-Lagrangian approach in industrial applications, the Eulerian-Eulerian approach is the most frequently used. This approach assumes the gas-solid phases as continuous and fully interpenetrating within each control volume, and use the Kinetic Theory of Granular Flow (KTGF) to describe the stress tensor in the solid momentum equation, allowing a more realistic representation for particle-particle interactions, providing variables such as shear and bulk viscosity, as well as a solid pressure (Syamlal, Rogers, and O'Brien 1989; Reuge et al., 2008).

In the Eulerian-Eulerian approach, the gas-solid flow hydrodynamics strongly depends on the description of the interphase momentum transfer between the gas and solid phases which is one of the dominant forces in the gas-solid phase momentum balances. This momentum exchange is accounted by using a drag model. Thus, the predictive accuracy of a CFD model depends on the drag model used (Taghipour et al., 2005; Du et al., 2006; Sobieski, 2009; de Souza Braun et al., 2010; Esmaili and Mahinpey 2011).

Due to diverse applications of gas-solid flow systems, many drag models have been proposed in literature. According to Tenneti et al. (2011) many drag models that are widely used in engineering practice are either obtained from pressure drop measurements in packed beds or measurements of terminal velocity in sedimenting suspensions. Thus, several studies have been conducted in order to identify which drag models to predict more accurately the gas-solid flow hydrodynamics in a fluidized bed at diverse regimes (Du et al., 2006; Vejahati et al., 2009; Esmaili & Mahinpey, 2011; Loha et al., 2012). However, there is no agreement among the various studies involving drag models.

The literature also reported drag model derived from direct numerical simulation technique (Hill et al., 2001; van der Hoef et al., 2005 and Beetstra et al., 2007). These drag models were established by direct numerical simulation technique the Lattice-Boltzmann (LB) simulation. The advantage of this kind of simulation is that the flow conditions and the material itself can be perfectly controlled, which is often not the case of experiments (Gryczka et al., 2009).

As appointed by Wang et al. (2010) the drag models derived from Lattice Boltzmann simulations may be more accurate than the models obtained from experiments. According to Esmaili and Mahinpey (2011) the works of van de Hoef et al., (2005) e Beetstra et al., (2007) proposed expressions for normalized drag force for both mono-dispersed and poly-dispersed systems. Their results found to be in excellent agreement (deviation smaller than 3%) with the simulation data of several models proposed in literature.

Nevertheless, even if these drag models have successfully got better results in specified cases, they should be further validated for wide applications. Though there have been published studies involving different drag models, there are few studies concerning the drag models derived from Lattice Boltzmann simulations applied to CFD studies of bubbling fluidized beds.

The objective of this work is to provides a comprehensive study of these drag models derived from Lattice Boltzmann simulations, in order to assess their performance in simulating gas-solid flow hydrodynamics in a bubbling fluidized bed. Moreover, the Gidaspow (1994) drag model was considered in order to compare the prediction obtained by LB drag models. A CFD model using the MFIX code based on the Eulerian-Eulerian approach used along with KTGF was used to simulate a 2D bubbling fluidized bed with Geldart B particles. The results are validated with the experimental data from Jung et al. (2005).

2. HYDRODYNAMIC MODELING

In the Eulerian-Eulerian approach the conservation equations for the solid and gas phase are solved individually and closed with the appropriate constitutive equations. The continuity equations for the gas (g) and solid (s) phases can be written as:

$$\frac{\partial}{\partial t}(\alpha_g \rho_g) + \nabla(\alpha_g \rho_g \vec{u}_g) = 0 \tag{1}$$

$$\frac{\partial}{\partial t}(\alpha_s \rho_s) + \nabla(\alpha_s \rho_s \vec{u}_s) = 0 \tag{2}$$

The momentum equations for the gas and solid phases are given as follow:

$$\frac{\partial}{\partial t}(\alpha_g \rho_g \vec{u}_g) + \nabla(\alpha_g \rho_g \vec{u}_g \vec{u}_g) = \alpha_g \vec{\nabla} \overline{\overline{\sigma}}_g - \vec{F}_D + \alpha_g \rho_g \vec{g} \tag{3}$$

$$\frac{\partial}{\partial t}(\alpha_s \rho_s \vec{u}_s) + \nabla(\alpha_s \rho_s \vec{u}_s \vec{u}_s) = \vec{\nabla} \overline{\overline{\sigma}}_s + \alpha_s \vec{\nabla} \overline{\overline{\sigma}}_g + \vec{F}_D + \alpha_s \rho_s \vec{g} \tag{4}$$

Where, α_k and u_k are the volumetric fractions and local temporal velocity vectors (m/s) of *k* phase, respectively; $\overline{\overline{\sigma}}_k$ stands for the k phase stress tensor (Pa). $\vec{F}_D$ represents the momentum transfer between the gas and solid phases (N/m^3) and is commonly expressed as $\vec{F}_D = \beta_{gs}(\vec{u}_g - \vec{u}_s)$, where β_{gs} is the drag model. $\vec{g}$ is the gravitational constant force (m/s^2).

Under regime dense flow conditions, the gas-phase turbulent stresses could be neglected without any appreciable effect on the time-averaged flow profiles. For the gas phase, the stress tensor, $\overline{\overline{\sigma}}_g$, and shear stress, $\overline{\overline{\tau}}_g$, are given by equations (5) and (6), respectively:

$$\overline{\overline{\sigma}}_g = -p_g \overline{\overline{I}} + \overline{\overline{\tau}}_g \tag{5}$$

$$\overline{\overline{\tau}}_g = \mu_g \left[\nabla \vec{u}_g + (\nabla \vec{u}_g)^T - \frac{2}{3} \nabla \vec{u}_g \overline{\overline{I}} \right] \tag{6}$$

For the solid phase, Syamlal et al. (1993) has formulated a solid phase stress tensor, $\overline{\overline{\sigma}}_s$, combining the KTGF of Jenkins and Savage (1983) with the critical state theory of Schaeffer (1987) to model dilute and dense gas-solid flow, respectively. The combination of both theories for viscous and plastic flow regimes was applied to investigate the behavior of granular flow, respectively, leading to the following relations for computing the solid phase stress constitutive equations, represented as:

$$\overline{\overline{\sigma}}_s = \begin{cases} -p_s^p \overline{\overline{I}} + \overline{\overline{\tau}}_s^p \rightarrow \alpha_g \le \alpha_g^* \\ -p_s^v \overline{\overline{I}} + \overline{\overline{\tau}}_s^v \rightarrow \alpha_g > \alpha_g^* \end{cases} \tag{7}$$

where, the upper indices (p) and (v) correspond to plastic and viscous regimes respectively, and α_g^* is the initial voidage in the bed. The solid phase stresses tensor in the plastic flow regime is described by theories from the study of solid mechanics. The solid phase pressure in a plastic regime is determined by:

$$p_s^p = \alpha_s p^* \tag{8}$$

where, p^* is represented by an empirical power law with typical values of $A = 10^{25}$ and $n = 10$

$$p^* = \alpha_s A(\alpha_g^* - \alpha_g)^n \tag{9}$$

The solid phase shear stress in the plastic regime is calculated as:

$$\overline{\overline{\tau}}_s^p = 2\mu_s^p \overline{\overline{D}}_s \tag{10}$$

where, μ_s^p is the solid phase dynamic viscosity in the plastic regime

$$\mu_s^p = \frac{p^* \sin \Phi}{2\sqrt{I_{2D}}} \tag{11}$$

where, Φ is an angle of internal friction and I_{2D} represents the second invariant of the deviator of the strain rate tensor D_s , is given by:

$$I_{2D} = \frac{1}{6}\left[(D_{s11} - D_{s22})^2 + (D_{s22} - D_{s33})^2 + (D_{s33} - D_{s11})^2 \right] + D_{s12}^2 + D_{s23}^2 + D_{s31}^2 \tag{12}$$

The solid phase stresses tensor in the viscous regime is calculated using KTGF. Solid physical properties such as, p_s^v , μ_s^v , λ_s^v are determined as a function of granular temperature, θ_s, represented as:

$$p_s^v = K_1 \alpha_s^2 \theta_s \tag{13}$$

$$\overline{\overline{\tau}}_s^v = 2\mu_s^v \overline{\overline{D}}_s + \lambda_s^v tr(\overline{\overline{D}}_s) \overline{\overline{I}} \tag{14}$$

where, μ_s^v and λ_s^v is the solid phase dynamic and volumetric viscosities in the viscous regime respectively, expressed by:

$$\mu_s^v = K_3 \alpha_s \sqrt{\theta_s} \tag{15}$$

$$\lambda_s^v = K_2 \alpha_s \sqrt{\theta_s} \tag{16}$$

In this work, the algebraic granular temperature equation was used. According to Syamlal et al. (1993), this allows the possibility of convergence acceleration by directly computing the granular temperature through a simple algebraic expression, instead of solving a complex partial differential equation (PDE). As appointed by Hosseini et al. (2010), the algebraic granular temperature equation can be reasonably used without diminishing its accuracy only when the gas-solid flow has higher values of solid volumetric fraction and lower values of solid velocity, such as in a dense regime. The algebraic granular temperature equation is represented as:

$$\theta_s = \left\{ \frac{-K_1 \alpha_s tr(\overline{\overline{D}}_s) + \sqrt{K_1^2 tr^2(\overline{\overline{D}}_s)\alpha_s^2 + 4\mathrm{K}_4 \alpha_s [K_2 tr^2(\overline{\overline{D}}_s) + 2\mathrm{K}_3 tr^2(\overline{\overline{D}}_s)]}}{2\mathrm{K}_4 \alpha_s} \right\}^2 \tag{17}$$

where, K_1, K_2, K_3 and K_4 are defined as:

$$K_1 = 2(1+e)\rho_s g_0 \tag{18}$$

$$K_2 = \frac{4 \mathrm{d}_s \rho_s (1+e) \alpha_s g_0}{3\sqrt{\pi}} - \frac{2}{3} K_3 \tag{19}$$

$$K_3 = \frac{d_s \rho_s}{2} \left\{ \frac{\sqrt{\pi}}{3(3-e)} [1 + 0{,}4(1+e)(3e-1)\alpha_s g_0] + \frac{8\alpha_s g_0 (1+e)}{5\sqrt{\pi}} \right\} \tag{20}$$

$$K_4 = \frac{12(1-e^2)\rho_s g_0}{d_s \sqrt{\pi}} \tag{21}$$

Finally, e is the restitution coefficient, this variable represent the collisions of solid particles, and g_0 is the radial distribution function in contact with solid particles. The MFIX code uses by default the Carnahan and Starling (1969) radial distribution function defined by:

$$g_0 = \frac{1}{\alpha_g} + \frac{1{,}5\alpha_g}{\alpha_g^2} \tag{22}$$

2.1 Lattice Boltzmann drag models

The Hill et al., (2001) drag model was developed based on a number of different formulas for the drag function at different Reynolds numbers and particle volume fractions.

$$\beta_{gs} = 18\mu_g (1-\alpha_s)^2 \alpha_s \frac{F}{d_s^2} \tag{23}$$

where F is variable defined as:

$$F = 1 + 3/8\,\mathrm{Re}_s \quad \alpha_s \le 0.01 \quad and \quad \mathrm{Re}_s \le (F_2 - 1)/(3/8) - F_3$$
$$F = F_0 + F_1 \mathrm{Re}_s^2 \quad \alpha_s > 0.01 \quad and \quad \mathrm{Re}_s \le F_3 + \sqrt{F_3^2 - 4F_1(F_0 - F_2)}\,/\,2F_1 \tag{24}$$
$$F = F_2 + F_3 \mathrm{Re}_s \begin{cases} \alpha_s \le 0.01 \quad and \quad \mathrm{Re}_s > (F_2 - 1)/(3/8) - F_3 \\ \alpha_s > 0.01 \quad and \quad \mathrm{Re}_s > F_3 + \sqrt{F_3^2 - 4F_1(F_0 - F_2)}\,/\,2F_1 \end{cases}$$

In which the parameters are defined as follows:

$$F_0 = \begin{cases} (1-w)\left[\dfrac{1 + 3\sqrt{\alpha_s/2} + (135/64)\alpha_s \ln(\alpha_s) + 17.41\alpha_s}{1 + 0.681\alpha_s - 8.4\alpha_s^2 + 8.16\alpha_s^3}\right] + w\left[10\alpha_s/(1-\alpha_s)^3\right] & 0.01 < \alpha_s < 0.4 \\ \dfrac{10\alpha_s}{(1-\alpha_s)^3} \quad \alpha_s > 0.4 \end{cases} \tag{25}$$

$$F_1 = \begin{cases} \dfrac{\sqrt{(2/\alpha_s)}}{40} & 0.01 < \alpha_s \le 0.1 \\ 0.11 + 0.00051 e^{(11.6\alpha_s)} & \alpha_s > 0.1 \end{cases} \tag{26}$$

$$F_2 = \begin{cases} (1-w)\left[\dfrac{1 + 3\sqrt{\alpha_s/2} + (135/64)\alpha_s \ln(\alpha_s) + 17.89\alpha_s}{1 + 0.681\alpha_s - 11.03\alpha_s^2 + 15.41\alpha_s^3}\right] + w\left[10\alpha_s/(1-\alpha_s)^3\right] & \alpha_s < 0.4 \\ \dfrac{10\alpha_s}{(1-\alpha_s)^3} \quad \alpha_s \ge 0.4 \end{cases} \tag{27}$$

$$F_3 = \begin{cases} 0.9351\alpha_s + 0.03667, & \alpha_s < 0.0953 \\ 0.0673 + 0.212\alpha_s + 0.0232/(1-\alpha_s)^5, & \alpha_s \ge 0.0953 \end{cases} \tag{28}$$

$$\mathrm{Re}_s = \frac{\rho_g d_s (1-\alpha_s)\left|u_g - u_s\right|}{2\mu_g} \tag{29}$$

$$w = e^{(-10(0.4-\alpha_s)/\alpha_s)} \tag{30}$$

The Van de Hoef et al., (2005) drag model was derived for the case of static arrays of particles under steady state conditions at low Reynolds numbers.

$$\beta_{gs} = \frac{18\mu_g (1-\alpha_s)^2 \alpha_s}{d_s^2}\left(F_0(\alpha_s) + F_1(\alpha_s)\mathrm{Re}_s\right) \tag{31}$$

In which dimensionless coefficients $F_0(\alpha_s)$, $F_1(\alpha_s)$ and Re_s are defined as:

$$F_0(\alpha_s) = 10\frac{\alpha_s}{(1-\alpha_s)^2} + (1-\alpha_s)^2(1 + 1.5\sqrt{\alpha_s}) \tag{32}$$

$$F_1(\alpha_s) = \frac{0.48 + 1.9\alpha_s}{18(1-\alpha_s)^2} \tag{33}$$

$$\mathrm{Re}_s = \frac{\rho_g |u_g - u_s| d_s}{\mu_g} \tag{34}$$

Beetstra et al., (2007) drag model is slightly more accurate than the Hill et al. (2001) drag model because it is based on a wider range of Reynolds numbers. The particles were given a constant velocity in some arbitrary direction so that the array of spheres was moving as a static configuration through the system.

$$\beta_{gs} = \frac{18\mu_g (1-\alpha_s)^2 \alpha_s}{d_s^2} F_0 \tag{35}$$

In which F_0 takes the form:

$$F_0 = 10\frac{\alpha_s}{(1-\alpha_s)^2} + (1-\alpha_s)^2(1+1.5\sqrt{\alpha_s}) + \frac{0.413\mathrm{Re}_s}{24(1-\alpha_s)^2}\left[\frac{(1-\alpha_s)^{-1} + 3\alpha_s(1-\alpha_s) + 8.4\mathrm{Re}_s^{-0.343}}{1+10^{3\alpha_s}\mathrm{Re}_s^{-(1+4\alpha_s)/2}}\right] \tag{36}$$

2.2 Empirical drag models

The Gidaspow (1994) drag model combines the Ergun equation and the Wen-Yu drag model in order to describe gas-solid flow hydrodynamics in dense and dilute phases.

$$\beta_{gs} = 150\frac{\alpha_s^2 \mu_g}{\alpha_g d_s^2} + 1.75\frac{\alpha_s \rho_g |u_g - u_s|}{d_s}, \quad \alpha_g < 0.8 \tag{37}$$

$$\beta_{gs} = \frac{3}{4} C_D \frac{\alpha_s \alpha_g \rho_g |u_g - u_s|}{d_s} \alpha_g^{-2.65}, \quad \alpha_g > 0.8 \tag{38}$$

$$C_D = \begin{cases} \frac{24}{\alpha_g \mathrm{Re}_s}\left[1 + 0.15(\alpha_g \mathrm{Re}_s)^{0.687}\right] & \mathrm{Re}_s \le 1000 \\ 0.44 \quad \mathrm{Re}_s > 1000 \end{cases} \tag{39}$$

$$\mathrm{Re}_s = \frac{\rho_g |u_g - u_s| d_s}{\mu_g} \tag{40}$$

3. NUMERICAL SOLUTION PROCEDURE

Open source MFIX code version 2012-1 was used to carry out a set of simulations of gas-solid flow in a 2D bubbling fluidized bed considering a Cartesian framework, as shown in Fig. 1. In most of the previous studies, 2D Eulerian-Eulerian simulations have been used essentially to minimize computational requirements.

A grid size of 5.0mm was selected to reduce computational resources, according to Esmaili and Mahinpey (2011), this grid size makes it possible to forecast hydrodynamics in a reasonably efficient amount of time without sacrificing the accuracy of results. The van der Hoef et al. (2005) drag model was implemented in the MFIX code, the other drag models are already implemented. The operating conditions, gas and solid properties used in the experimental setup of Jung et al. (2005) are summarized in Table 1. The work of Jung et al., (2005) shows a solid-velocity profile in the radial direction at a height of 0.14. This experimental result will be used to assess the prediction of solid-velocity profile in the radial direction by each drag model. The simulations were performed for a time period of 20 seconds. Nevertheless, to avoid the large time-related instability of all the variables in the early seconds of the simulation, time was averaged between 5 – 20 seconds in a real-time simulation. The SUPERBEE scheme was used in this study. A fixed time step at the 10^{-5} order of magnitude is enough to avoid the instability in convergence in 2D simulations. The left and right walls of the fluidized bed were treated as if they were no-slip boundaries for both phases, while at the bottom of the fluidized bed, a uniform gas inlet velocity was specified and atmospheric pressure was set at the top of the freeboard.

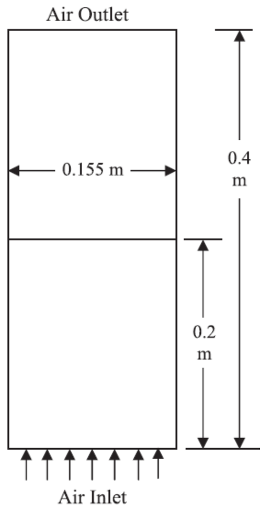

Fig. 1. Schematic of bubbling fluidized bed reactor.

Table 1. Properties of the gas and solid phase from Jun et al. (2005).

Bed width	0.155 m
Bed height	0.4 m
Static bed height	0.2 m
Particle density (glass beads)	2500 kg/m^3
Mean particle diameter	530 µm
Initial solids packing	0.4
Restitution coefficient	0.99
Air density	1.225 kg/m^3
Air viscosity	1.8×10^{-5} kg/m.s
Superficial gas velocity	0.587 m/s

4. RESULTS AND DISCUSSION

Figure 2 illustrates the comparison of time-averaged axial solid particle profile in the radial direction at a height of 0.14 m between the simulation results using different drag models and the experimental result performed by Jung et al. (2005). The simulation results show the existence of core-annular structure of the flow, consisting of a central region in which the solid particles are carried up by the gas and an annular region where particle fall down along the wall, are clearly predicted by LB drag models.

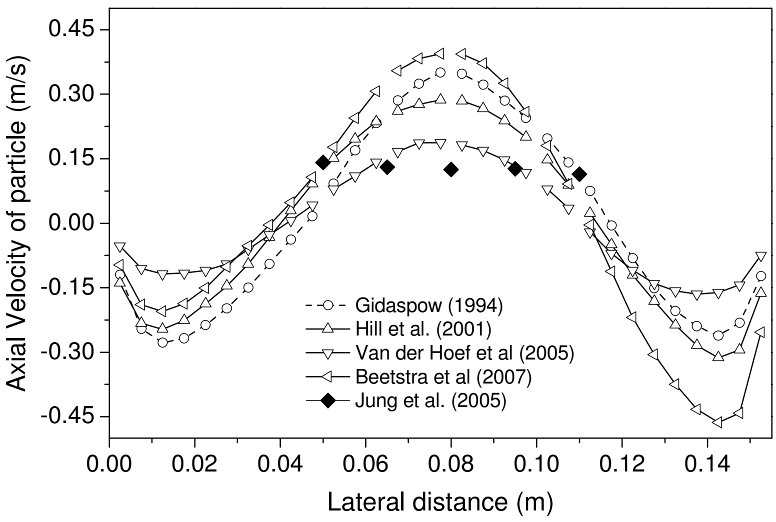

Fig. 2. Time-averaged particle axial velocity profile along the radial direction at h=0.14m

Gidaspow (1994), Hill et al. (2001) and Beetstra et al. (2007) drag models over predict the velocity near the central region. However, the van der hoef et al. (2005) drag model matches very well with the experimental time-averaged particle velocity available at the central region of the bed. Beetstra et al. (2007) e Gidaspow (1994) drag models predict the higher speeds of the solid particles, specifically in central bed and a wide circulation of particles on the walls of the fluidized bed.

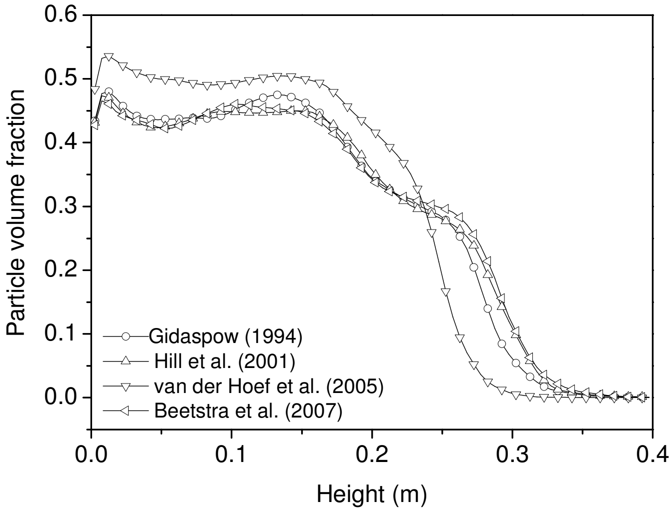

Fig. 3. Time-averaged solid volume fraction variation along the central axis.

Figure 3 shows the time-averaged solid volume fraction variation along the central axis. It can be seen that the volume fraction provided by Gidaspow (1994), Hill et al. (2001) e Beetstra et al. (2007) drag models showed almost no change in time-averaged solid volume fraction variation in the axial direction. However, van der Hoef et al. (2005) drag model shows a different trend being a little smaller compared to the other designs, the same observed in predicting the speed of the solid particles. The volume fraction of particles is decreasing along the bed height , this due to the passage of bubbles within the bed. Through this profile, one can obtain a primary notion of the expected expansion of the bed through the drag models.

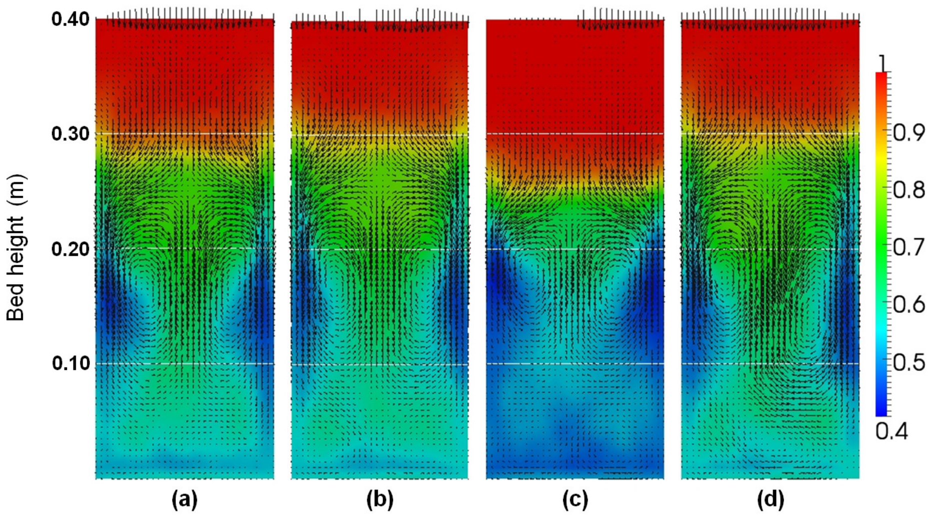

Fig. 4. Time-averaged voidage distribution and particle velocity vector (a) Gidaspow (1994); (b) Hill et al. (2001); (c) van der Hoef et al. (2005) and Beetstra et al. (2007).

Figure 4 shows the time-averaged voidage distribution and particle velocity vector of different drag models at superficial gas velocities of 0.587 m/s. The time-averaged voidage distributions gives an overview of the allocation of solid particles in the bed so that their concentration can be estimated, where the color scale represents the voidage fraction scale. The blue color corresponds to a voidage of 0.40 and the red color corresponds to voidage of 1. The vectors indicate the direction of the particles.

All the models can represent a similar behavior, which is characterized by increased voidage caused by the passage of bubbles within the fluidized bed. Furthermore, by vector particle can identify the particle vorticity forming the top of the bed near the freeboard. Whereas the initial height of the fixed bed 0.20m, from Fig. 4 it is observed that all drag models predict a clear bed expansion. Among all the forecasts the van der Hoef et al. (2005) drag model has the lowest bed expansion. In addition, the simulation result demonstrates the presence of high concentration of solids zones, particularly the walls of the fluidized bed. This confirms the particle velocity profiles where higher speeds are attained in the central part of the bed and that there is a large movement of particles on the walls of the fluidized bed.

5. CONCLUSIONS

The drag models derived from Lattice Boltzmann simulations reported by Hill et al. (2001), van der Hoef et al. (2005) and Beetstra et al. (2007) reported in the literature was studies. All LB drag models showed an acceptable qualitative agreement with the experimental data. Most drag models overestimate the particle velocity within the bed, however, the van der Hoef et al. (2005) drag model was the one with the best forecast. The most widely used drag model (Gidaspow's drag model) was compared to the LB drag models. From the results it can be concluded that the LB drag models has the same ability to predict the gas-solid hydrodynamics in a bubbling fluidized bed that drag models obtained from experimental tests. As computer technology improves, more accurate drag models are expected to be developed based on the Lattice Boltzmann (LB) simulation.

6. ACKNOWLEDGEMENTS

The authors are grateful to National Council of Technological and Scientific Development (CNPq) process (150894/2014-7) and São Paulo Research Foundation (FAPESP) process (2013/21244-5).

7. REFERENCES

L.M. Armstrong, S. Gu, K.H. Luo, Study of wall-to-bed heat transfer in a bubbling fluidised bed using the kinetic theory of granular flow, Int. J. Heat Mass Transf. 53 (2010) 4949–4959.

R. Beetstra, M. Van der Hoef, J. Kuipers, Drag force of intermediate Reynolds number flow past mono and bidisperse arrays of spheres, AIChE J. 53 (2007) 489–501.

W. Du, X. Bao, J. Xu, W. Wei, Computational fluid dynamics (CFD) modeling of spouted bed: Assessment of drag coefficient correlations, Chem. Eng. Sci. 61 (2006) 1401–1420.

M.P. de Souza Braun, A.T. Mineto, H.A. Navarro, L. Cabezas-Gómez, R.C. da Silva, The effect of numerical diffusion and the influence of computational grid over gas–solid two-phase flow in a bubbling fluidized bed, Math. Comput. Model. 52 (2010) 1390–1402.

E. Esmaili, N. Mahinpey, Adjustment of drag coefficient correlations in three dimensional CFD simulation of gas–solid bubbling fluidized bed, Adv. Eng. Softw. 42 (2011) 375–386.

D. Gidaspow, Multiphase Flow and Fluidization: Continuum and Kinetic Theory Description, Academic Press, San Diego, 1994.

O. Gryczka, S. Heinrich, N.G. Deen, M. van Sint Annaland, J. a. M. Kuipers, M. Jacob, et al., Characterization and CFD-modeling of the hydrodynamics of a prismatic spouted bed apparatus, Chem. Eng. Sci. 64 (2009) 3352–3375.

C.K. Gupta, D. Sathiyamoorthy, Fluid Bed Technology in Materials Processing, CRC Press, Boca Raton, 1999.

R.J. Hill, D.L. Koch, A.J.C. Ladd, Moderate-Reynolds-number flows in ordered and random arrays of spheres, J. Fluid Mech. 448 (2001) 243–278.

S.H. Hosseini, W. Zhong, M.N. Esfahany, L. Pourjafar, S. Azizi, CFD Simulation of the Bubbling and Slugging Gas-Solid Fluidized Beds, J. Fluids Eng. 132 (2010) 041301.

J. Jung, D. Gidaspow, I.K. Gamwo, Measurement of Two Kinds of Granular Temperatures, Stresses, and Dispersion in Bubbling Beds, Ind. Eng. Chem. Res. 44 (2005) 1329–1341.

D. Kunii, O. Levenspiel, Fluidization Engineering, second ed, Butterworths, London, 1991.

S. Oka, E.J. Anthony, Fluidized Bed Combustion, 2004.

C. Loha, H. Chattopadhyay, P.K. Chatterjee, Assessment of drag models in simulating bubbling fluidized bed hydrodynamics, Chem. Eng. Sci. 75 (2012) 400–407.

M. Schreiber, T.W. Asegehegn, H.J. Krautz, Numerical and experimental investigation of bubbling gas–solid fluidized beds with dense immersed tube bundles, Ind. Eng. Chem. Res. (2011) 7653–7666.

M.T. Shah, R.P. Utikar, M.O. Tade, G.M. Evans, V.K. Pareek, Effect of a cluster on gas-solid drag from lattice Boltzmann simulations, Chem. Eng. Sci. 102 (2013) 365–372

W. Sobieski, Momentum exchange in solid–fluid system modeling with the Eulerian multiphase model, Dry. Technol. 27 (2009) 653–671.

M. Syamlal, T.J. O'Brien, Computer simulation of bubbles in a fluidized bed, AIChE Symp. 85 (1989) 22–31.

M. Syamlal, W. Rogers, T.J. O'Brien, MFIX Documentation: Volume 1, Theory Guide. National Technical Information Service, Springfield, 1993.

S. Tenneti, R. Garg, S. Subramaniam, Drag law for monodisperse gas-solid systems using particle-resolved direct numerical simulation of flow past fixed assemblies of spheres, Int. J. Multiph. Flow. 37 (2011) 1072–1092

M.V. der a. Van Der Hoef, R. Beetstra, J. a. M. Kuipers, Lattice-Boltzmann simulations of low-Reynolds-number flow past mono- and bidisperse arrays of spheres: results for the permeability and drag force, J. Fluid Mech. 528 (2005) 233–254.

F. Vejahati, N. Mahinpey, N. Ellis, M.B. Nikoo, CFD simulation of gas-solid bubbling fluidized bed: A new method for adjusting drag law, Can. J. Chem. Eng. 87 (2009) 19–30.

V. Verma, N.G. Deen, J.T. Padding, J. a M. Kuipers, Two-fluid modeling of three-dimensional cylindrical gas-solid fluidized beds using the kinetic theory of granular flow, Chem. Eng. Sci. 102 (2013) 227–245. doi:10.1016/j.ces.2013.08.002.

J. Wang, M. a. van der Hoef, J. a M. Kuipers, CFD study of the minimum bubbling velocity of Geldart A particles in gas-fluidized beds, Chem. Eng. Sci. 65 (2010) 3772–3785.

S. Zimmermann, F. Taghipour, CFD modeling of the hydrodynamics and reaction kinetics of FCC fluidized-bed reactors, Ind. Eng. Chem. Res. 44 (2005) 9818–9827.

8. RESPONSIBILITY NOTICE

The authors are the only responsible for the printed material included in this paper.